Journal of Mineralogical and Petrological Sciences, Volume 112, page 77–87, 2017

Pressure–temperature–time path of a metapelite from Mefjell, Sør Rondane Mountains, East Antarctica

Yumiko TSUBOKAWA[*], Masahiro ISHIKAWA[*], Tetsuo KAWAKAMI[**], Tomokazu HOKADA[***], M. SATISH-KUMAR[†], Noriyoshi TSUCHIYA[‡] and Geoffrey H. GRANTHAM[§]

[*]*Graduate School of Environment and Information Sciences, Yokohama National University, Yokohama 240–8501, Japan*
[**]*Department of Geology and Mineralogy, Graduate School of Science, Kyoto University, Kyoto 606–8502, Japan*
[***]*National Institute of Polar Research, Tokyo 190–8518, Japan*
[†]*Department of Geology, Faculty of Science, Niigata University, Niigata 950–2181, Japan*
[‡]*Graduate School of Environmental Studies, Tohoku University, Sendai 980–8579, Japan*
[§]*Department of Geology, University of Johannesburg, P.O. Box 524, Auckland Park, 2006, South Africa*

A metapelite preserving prograde and retrograde zoning in garnet from Mefjell, southern Sør Rondane Mountains (SRM), East Antarctica is described in detail and U–Th–Pb geochronological data are presented. Garnet, sillimanite, staurolite and biotite are in textural equilibrium in the matrix. The garnet shows three distinct compositional zones comprising core, mantle and rim. From core to the mantle, the spessartine content represents a bell-shaped profile. From mantle to the rim, spessartine content increases and pyrope decreases. Kyanite is present as tiny inclusions in the garnet core. The core also contains aggregates of sillimanite with radial cracks around them, interpreted to have resulted from the inversion of kyanite. The prograde *P–T* path recorded in the garnet is heating to approximately 700 °C at 5.6 kbar with a slight increase in pressure. U–Th–Pb dating of monazite grains yields a large range of age distribution between 700 and 540 Ma. The inferred prograde metamorphism of the metapelite sample in this study might be related to subduction and/or tectonic loading explained by a collision tectonic model of the SRM (Osanai et al., 2013).

Keywords: East Antarctica, Sør Rondane Mountains, Pressure and temperature conditions, Prograde zoning

INTRODUCTION

The Sør Rondane Mountains (SRM) of eastern Dronning Maud Land, East Antarctica, have been considered to be an integral part of the continental collision zone of the East African–Antarctic Orogen (e.g. Jacobs and Thomas, 2004; Jacobs et al., 2015). Meert (2003) further recognized two main orogenies within eastern Gondwana including East Antarctica, referred to as the East Africa Orogen (EAO) and the Kuunga Orogen (KO). The study of Meert (2003) was based largely on geochronological data which showed a North–South oriented EAO (~ 750–620 Ma) overprinted in the south by a marginally younger East–West oriented KO (570–530 Ma). Grantham et al. (2008) supported the KO of Meert (2003) by proposing a collisional model between N and S Gondwana based on a review of lithological, geochronological, structural and metamorphic *P–T* data between southern Africa, DML, Antarctica and Sri Lanka. Both the EAO and the KO orogenies have contributed to the incremental amalgamation of Gondwana initially involving collision in EAO followed by collision in KO. The SRM are located in an area where the EAO and KO intersect, having been affected by both orogenic phases.

The SRM are underlain by Neoproterozoic granulite facies and amphibolite facies metamorphic rocks, together with Neoproterozoic to lower Cambrian granitic rocks forming minor dikes and small plutons (Fig. 1, Shiraishi et al., 2008). The majority of the metamorphic rocks are intermediate in composition, represented by biotite–hornblende gneiss, with subordinate amounts of pelitic, calcareous, quartzo–feldspathic, mafic, and ultramafic rocks (Asami et al., 1992; Osanai et al., 1992; Grantham et al., 2013). Metamorphic ages of ~ 640–600 and ~ 550–500 Ma have been reported from the SRM (Shiraishi et

doi:10.2465/jmps.160919
Y. Tsubokawa, tsubokawa-yumiko-nd@ynu.jp Corresponding author

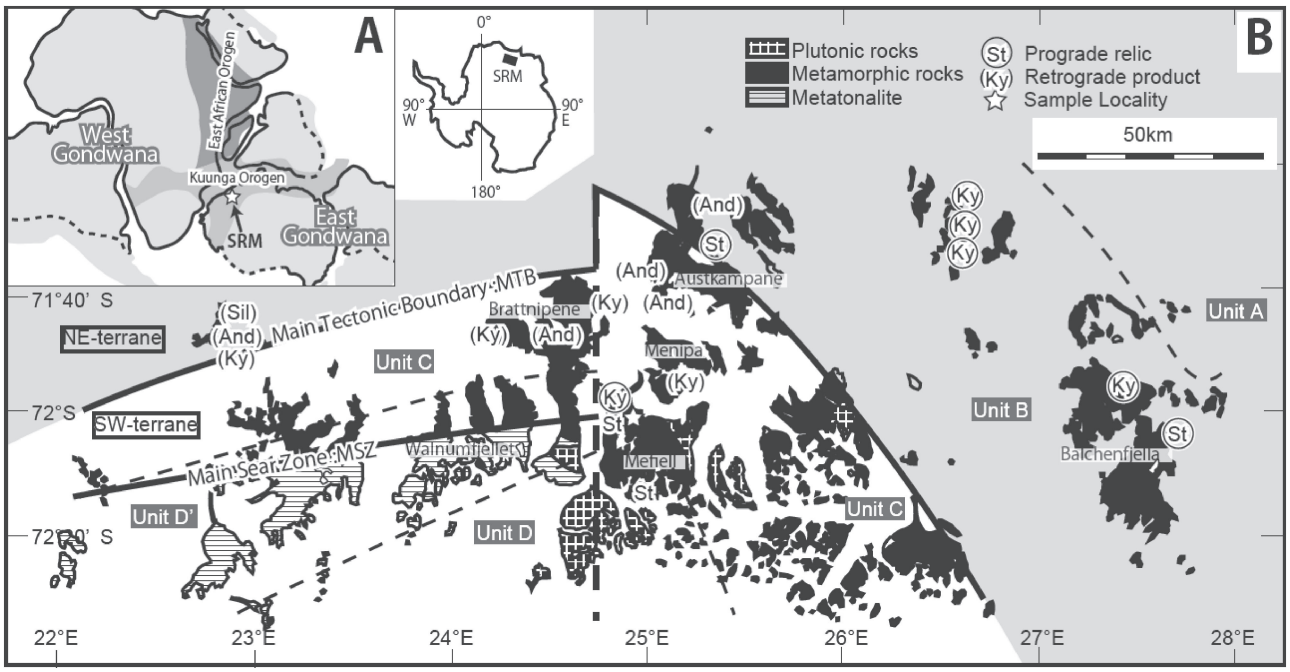

Figure 1. (A) Location of the Sør Rondane Mountains in a reconstruction of Gondwana. SRM are located in both the East African–Antarctic Orogen (Jacobs and Thomas, 2004) and the Kuunga Orogen (Meert, 2003). (B) Simplified geological map and proposed subdivisions of NE- and SW-terranes in the Sør Rondane Mountains (see Osanai et al., 2013). Location of MTB is after Osanai et al. (2013). Key minerals used in understanding the metamorphic evolution are indicated (Asami et al., 2007; Osanai et al., 2013; Kawakami et al., 2017). The studied sample was collected from Mefjell indicated by the white star.

al., 2008; Adachi, 2010). The metamorphic rocks record different *P–T* paths for the NE terrane and the SW terrane of the SRM (Osanai et al., 2013). The metamorphic rocks from the northern and eastern parts e.g., in Balchenfjella and northern Austkampane, reached peak conditions (760–800 °C, 7–8 kbar and 800 °C, 5–6 kbar, respectively) after decompression, and were followed by decompression and cooling, indicating clockwise *P–T* paths (Asami et al., 2007; Kawakami et al., 2010; Nakano et al., 2011; Adachi et al., 2013; Grantham et al., 2013; Higashino et al., 2013). In contrast, metamorphic rocks from the central SRM such as Brattnipene and Menipa reached peak conditions (900 °C, 6–7 kbar and 800 °C, 6 kbar) after compression, and were followed by nearly isobaric cooling, indicating anti-clockwise *P–T* paths (Owada et al., 2008; Adachi et al., 2013; Baba et al., 2013). An anti-clockwise *P–T* path has been reported from the western SRM recently (Perlebandet; Kawakami et al., 2017). However, the prograde metamorphic path of Mefjell is unclear. In order to attain more detailed discussions on the metamorphic evolution of SRM, it is important to recognize the variation in prograde *P–T* path within the same terrane.

In this paper, we describe a garnet porphyroblast in a metapelite from Mefjell preserving prograde chemical zoning and containing aluminosilicate inclusions, and also report U–Th–Pb geochronological results for the metapelite. Based on the results, we discuss the *P–T–t* evolution of the Mefjell region and compare these with existing models on the tectonic evolution of the SRM.

SAMPLE DESCRIPTION

The metapelite sample used in this study was obtained from northwestern Mefjell in the Unit D, in the SW terrane of the SRM (Fig. 1) during the summer season of the 51st Japan Antarctic Research Expedition (JARE 51; Tsuchiya et al., 2012). Mefjell is mainly composed of tonalitic gneiss and granite with minor metapelite and amphibolite. The matrix of the metapelite (sample MI09121202) consists mainly of garnet, sillimanite, biotite, plagioclase and quartz with minor amounts of staurolite, K-feldspar, apatite, ilmenite, magnetite, monazite and zircon (Fig. 2A). Chlorite is observed as a secondary mineral after biotite. Biotite and staurolite also occur as inclusions in garnet and plagioclase. Porphyroblastic garnet (12 mm in diameter) contains inclusions of kyanite, staurolite, sillimanite, biotite, ilmenite, hematite, magnetite, plagioclase, K-feldspar and quartz (Fig. 3). Ilmenite with exsolution lamellae of hematite is recognized as an inclusion in the garnet. The garnet shows zoning involving a change of color from reddish in the core to colorless

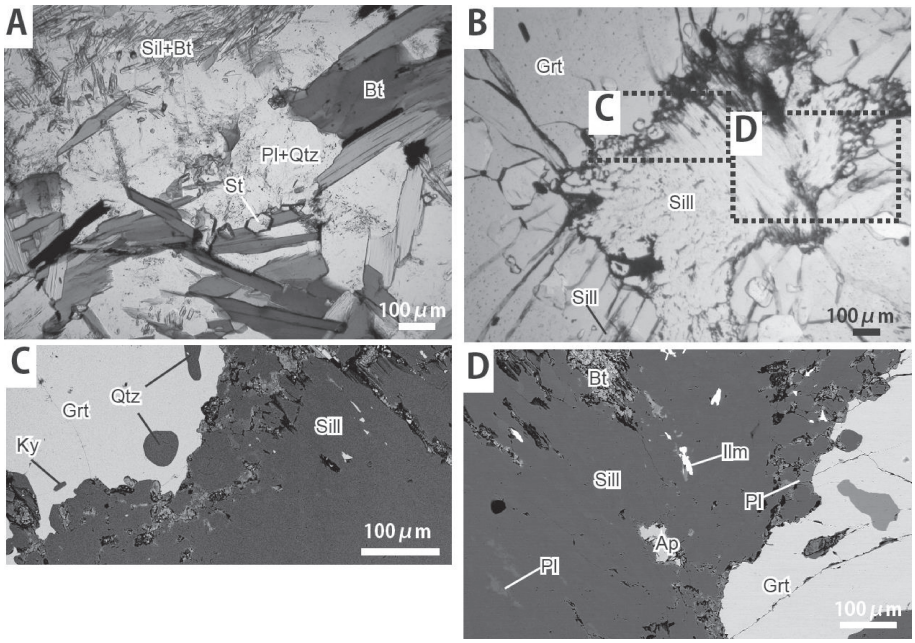

Figure 2. (A) Photomicrograph showing the mineral relationships in the metapelite. Sillimanite, staurolite and biotite are in textural equilibrium in the matrix. (B) Photomicrograph of sillimanite inclusion of boxed area in Figure 3 showing radial cracks around the sillimanite. (C) Backscattered electron image (BEI) of kyanite inclusion in the garnet core. (D) BEI of plagioclase inclusion and biotite inclusion in the garnet core. Color version of Figure 2 is available online from http://doi.org/10.2465/jmps.160919.

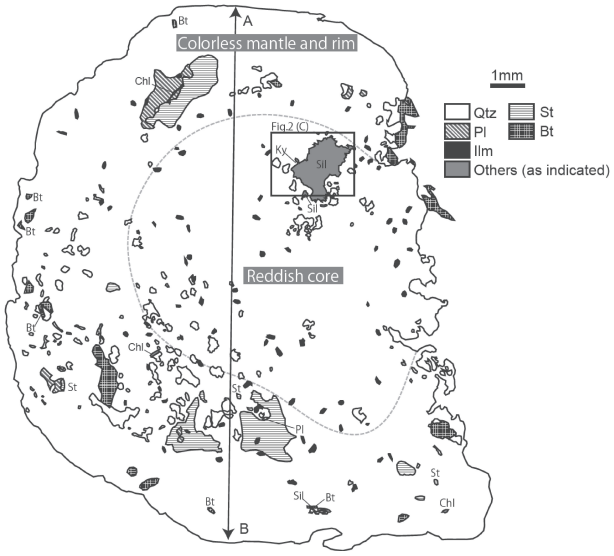

Figure 3. Distribution of mineral inclusion species in a garnet porphyroblast. Line AB indicates profile line of Figure 5.

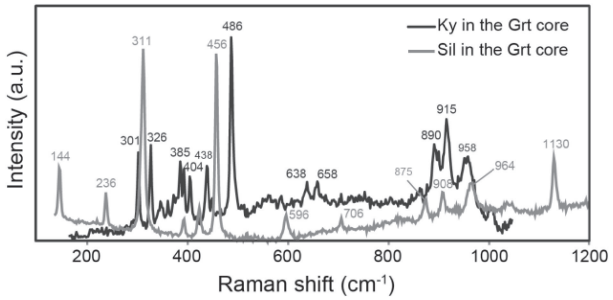

Figure 4. Representative Raman spectra for a sillimanite inclusion and a kyanite inclusion in the garnet core.

in the mantle and rim. Kyanite occurs as tiny inclusions only in the garnet core, confirmed by Raman spectroscopy (Figs. 2C and 4). Sillimanite included in the garnet exhibits two distinct microtextures: (1) fine-grained sillimanite aggregates in the garnet core with radial cracks around them, implying volume increase during the kyanite/sillimanite secondary polymorphic transition (Fig. 2B), (2) sillimanite crystals in the garnet mantle without radial cracks, indicating primary crystallization of sillimanite. Plagioclase occurs in the garnet core, associated with or included in the sillimanite aggregates (Fig. 2D). Plagioclase also occurs in the garnet mantle. Biotite inclusions in the sillimanite aggregates are found in the garnet core. Biotite also occurs in the mantle and rim of the garnet. Staurolite inclusions are found in the garnet mantle.

MINERAL CHEMISTRY

The major element chemistry of minerals in the studied rock were determined using an electron microprobe analyzer (JEOL JSM-5300, JXA-8530F and JXA-8800M) at Yokohama National University and the University of Tokyo, Japan. Analyses were performed at a 15 kV accelerating voltage, 10, 15 and 12 nA current respectively, and a ZAF correction was applied. Mineral abbreviations are after Kretz (1983).

Garnet

The garnet shows prograde zoning with a decrease in

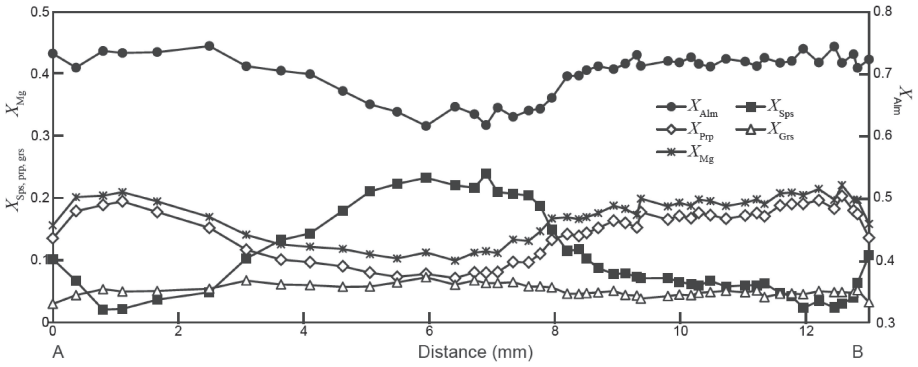

Figure 5. Compositional line profiles of the garnet porphyroblast along line AB (Fig. 3). Numbers represent mole fractions of the four end-member components and X_{Mg}.

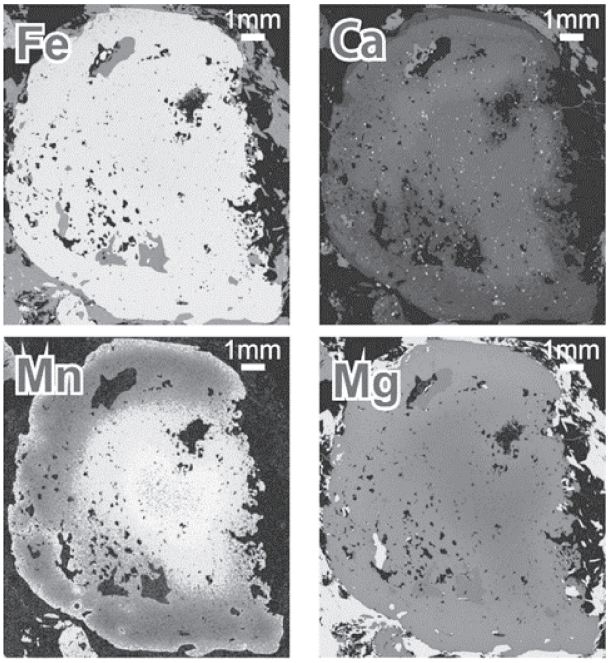

Figure 6. X-ray image map showing variations in Fe, Mn, Mg and Ca concentrations in the garnet.

spessartine content [X_{sps} = Mn/(Fe + Mg + Mn + Ca)] and increase in almandine [X_{alm} = Fe/(Fe + Mg + Mn + Ca)] and pyrope contents [X_{prp} = Mg/(Fe + Mg + Mn + Ca)] and in X_{Mg} [= Mg/(Mg + Fe)] from the core to the mantle (Figs. 5, 6, and Table 1). The spessartine content increases in the rim, indicating retrograde zoning effect. Results of X-ray Mn mapping suggest that the Mn-poor mantle is absent in some portions of the garnet, even though the garnet has the same Mn-enriched pattern in the rim. This variation in zoning might have resulted by preferential resorption after the mantle formation, and subsequent retrogression. Garnet also shows a slight increase in pyrope content and decrease in X_{Mg} towards contacts with biotite inclusions probably due to Fe-Mg exchange after entrapment. The grossular [X_{grs} = Ca/(Fe + Mg + Mn + Ca)] content is generally low throughout the garnet grain (Fig. 5).

Other minerals

Biotite grains in the matrix and those included in plagioclase show a relatively homogeneous X_{Mg} values with varying Ti content (TiO_2 = 1.2-2.2 wt%; X_{Mg} = 0.50-0.54) (Fig. 7). X_{Mg} values of biotite included in the mantle and in the rim of the garnet are different for each grain, and biotite in garnet is Mg-rich (X_{Mg} = 0.61-0.70) as compared with the matrix biotite and biotite in plagioclase (Fig. 7).

Plagioclase in the matrix shows chemical zoning with a decrease in anorthite content [X_{An} = Ca/(Ca + Na)] from the core (X_{An} = 33) to the rim (X_{An} = 23) (Fig. 8). Plagioclase in the garnet mantle has relatively homogeneous chemical compositions within each grain. Plagioclase inclusions in the garnet core and mantle have a slightly higher anorthite content (X_{an} = 27-38) compared with plagioclase in the garnet core (X_{an} = 26-27) and in the matrix.

Staurolite in the matrix and inclusions in the garnet mantle has higher X_{Mg} (X_{Mg} = 0.18-0.27), compared with staurolite inclusions in plagioclase (X_{Mg} = 0.16-0.22) (Fig. 9).

THERMOBAROMETRY

The *P-T* conditions were estimated from a garnet-biotite geothermometer (Holdaway, 2000) and a garnet-Al_2SiO_5-quartz-plagioclase geobarometer (Holdaway, 2001). The garnet core contains relict kyanite next to sillimanite presumably inverted from kyanite. Therefore, it can be assumed that even though *P-T* conditions might be close to those of the kyanite-sillimanite transition, the *P-T* path crossed from the kyanite to the sillimanite field when the garnet core grew. In contrast, the presence of sillimanite inclusions in the garnet mantle, as well as in the matrix, suggests that sillimanite was stable instead of kyanite during the peak to retrograde metamorphic conditions. The pre-peak metamorphic *P-T* conditions, estimated using the spessartine-enriched core composition of garnet, bio-

Table 1. Mineral composition of the metapelite

Stage	Pre-peak	Peak	Retrograde	Pre-peak	Peak	Peak	Retrograde	Pre-peak
Mineral	Grt			Pl		Pl		Bt
Mode of occurrence	In matrix			Inclusion in		In matrix		Inclusion in
	Core	Mantle	Rim	Grt core	Grt mantle	Core	Rim	Grt core
SiO_2	36.265	37.387	37.583	61.257	60.789	61.445	63.316	38.658
TiO_2	-	0.237	-	-	-	-	-	0.994
Al_2O_3	20.050	20.512	20.008	24.109	24.762	24.699	22.780	20.210
Cr_2O_3	-	-	-	-	-	-	-	-
FeO	27.957	33.095	32.650	0.721	-	-	0.534	14.003
MnO	10.429	1.361	4.827	-	-	-	-	0.380
MgO	1.989	5.261	3.446	-	-	-	-	14.774
CaO	2.573	1.751	1.133	5.879	6.939	6.414	4.564	-
Na_2O	-	0.384	-	7.758	7.168	7.237	8.453	0.578
K_2O	-	-	-	-	0.205	0.099	-	9.398
P_2O_5	-	-	-	-	-	-	0.187	-
Total	99.263	99.811	99.647	99.724	99.863	99.894	99.834	98.995
Number of O	12	12	12	8	8	8	8	22
Si	2.98	2.98	3.04	2.73	2.70	2.72	2.80	5.48
Ti	-	0.01	-	-	-	-	-	0.11
Al	1.94	1.93	1.91	1.27	1.30	1.29	1.19	3.38
Cr	-	-	-	-	-	-	-	-
Fe	1.92	2.21	2.21	0.03	-	-	0.02	1.66
Mn	0.73	0.09	0.33	-	-	-	-	0.05
Mg	0.24	0.63	0.42	-	-	-	-	3.12
Ca	0.23	0.15	0.10	0.28	0.33	0.30	0.22	-
Na	-	0.06	-	0.67	0.62	0.62	0.73	0.16
K	-	-	-	-	0.01	0.01	-	1.70
P	-	-	-	-	-	-	0.01	-
Total	8.05	8.07	8.00	4.97	4.96	4.95	4.96	15.65

Stage	Retrograde		
Mineral	Bt		
Mode of occurrence	In matrix		
	Core	Rim	In contact with Grt
SiO_2	38.411	39.118	36.338
TiO_2	1.844	1.774	1.716
Al_2O_3	19.237	19.621	19.171
Cr_2O_3	-	0.290	-
FeO	18.976	18.086	18.662
MnO	0.298	-	-
MgO	11.361	11.058	11.153
CaO	-	0.214	0.001
Na_2O	0.419	0.643	0.467
K_2O	9.394	9.102	9.637
P_2O_5	-	-	-
Total	99.940	99.906	97.145
Number of O	22	22	22
Si	5.52	5.58	5.40
Ti	0.20	0.19	0.19
Al	3.26	3.30	3.36
Cr	-	0.03	-
Fe	2.28	2.16	2.32
Mn	0.04	-	-
Mg	2.43	2.35	2.47
Ca	-	0.03	0.00
Na	0.12	0.18	0.14
K	1.72	1.66	1.83
P	-	-	-
Total	15.57	15.48	15.71

tite inclusion and plagioclase inclusion in sillimanite found in the garnet core, were 500 °C and 4.1 kbar. Peak metamorphic *P–T* conditions were estimated based on the pyrope-enriched mantle composition of garnet and plagioclase in the garnet mantle. We also use the composition of matrix biotite because biotite inclusions in the garnet mantle were probably affected by later Fe-Mg re-equilibration, inferred from an increase in Fe of the garnet in contact with biotite. The estimated peak conditions were 700 °C and 5.6 kbar. The garnet rim textures which implies resorption of garnet and its Mn-rich composition suggests consumption of garnet and the further growth of biotite during the retrograde stage. Consequently retrogressive conditions were estimated as 620 °C and 4.2 kbar using compositions analysed from the rim of garnet, rims of biotite in contact with garnet and rim of plagioclase in the matrix.

ELECTRON MICROPROBE DATING OF MONAZITE

We carried out U-Th-Pb dating for monazite using an electron probe micro analyzer (EPMA; JEOL JXA-8200) at the National Institute of Polar Research, Tokyo.

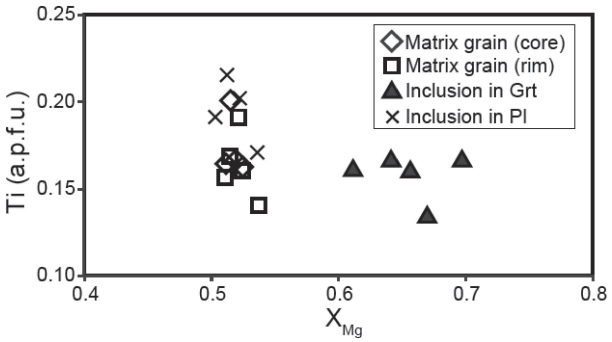

Figure 7. Compositional variations of biotite in terms of Ti (a.p.f.u., 22 oxygens) versus X_{Mg}.

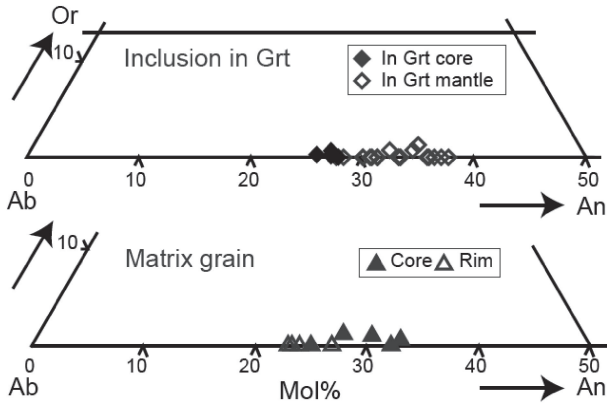

Figure 8. Ab–An–Or compositions of analyzed plagioclase.

The analytical and data reduction procedures are given in Hokada and Motoyoshi (2006).

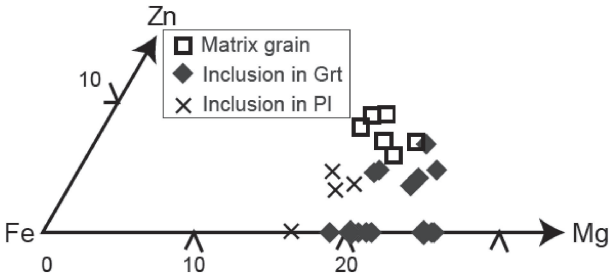

Figure 9. Chemical compositions of staurolite plotted on a Fe–Mg–Zn ternary diagram.

Monazite occurs in the matrix and as inclusions in biotite and plagioclase, and no monazite inclusions have been found in the garnet. Some grains preserve internal textures due to the difference in chemical composition (Fig. 10 and Table 2). A total of 37 analyses from 7 grains were obtained, which yielded ages ranging from 830 to 540 Ma (Fig. 11). The older ages (~ 830–740 Ma) are obtained from the inner brighter portion of matrix monazite, whereas there is no clear relationship between the ages and the analytical position within the grain for younger ages (700–540 Ma). If we assume a single 700–540 Ma population based on the histogram and probability density distribution, the younger ages define a weighted mean averaged age of 587 ± 14 Ma. The 840–740 Ma ages are scattered and it is difficult to define a specific event.

DISCUSSION

Relict kyanite is included in the garnet core next to the

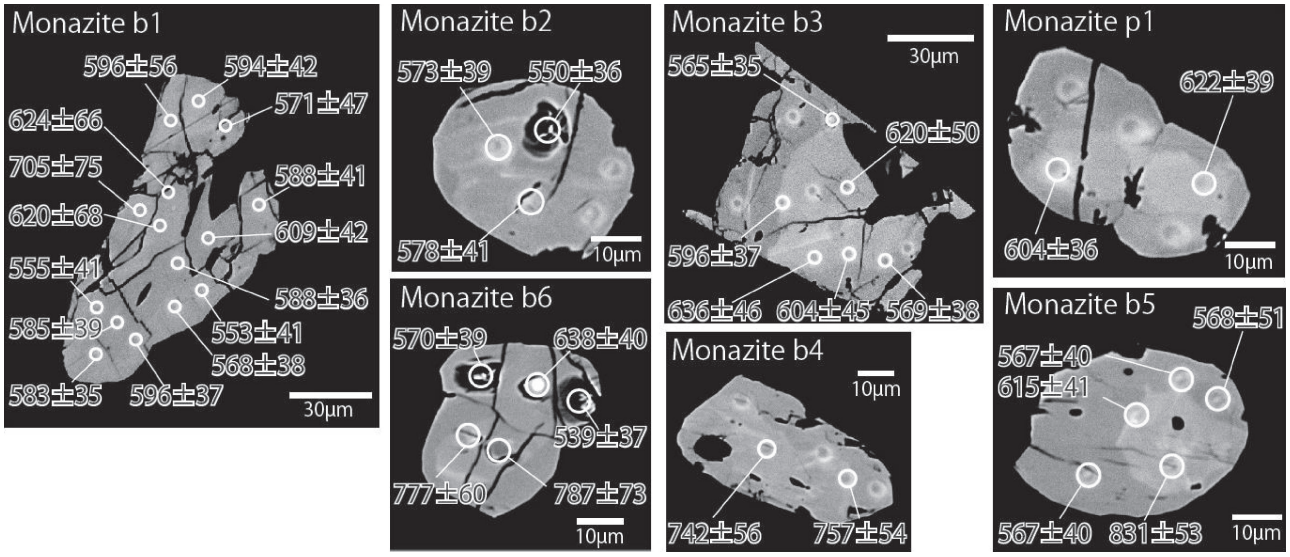

Figure 10. BSE images of representative analyzed monazite grains. U–Th–Pb monazite ages with 1-sigma error were plotted for each analysis spot. The small bright spots in the high-contrast BSE image of monazite show the analysis spot, and some holes were formed by a 5 μm electron beam. We excluded data with totals below 95 wt% from EPMA datae to improve the reliability of monazite ages.

Table 2. Representative chemical compositions and calculated age of monazite from sample MI09121202

Analyses no.	b1.1	b1.2	b1.3	b1.4	b1.5	b1.6	b1.7	b1.8	b1.9	b1.10	b1.11	b1.12
Mode of occurrence	Inclusion in Bt											
SiO_2	0.06	0.05	0.10	0.07	0.05	0.07	0.06	0.06	0.06	0.05	0.06	0.06
UO_2	1.18	1.64	0.78	0.58	0.67	0.60	1.15	1.48	1.46	1.44	1.54	1.56
ThO_2	4.07	2.01	3.35	3.03	2.25	2.84	4.11	3.32	4.55	3.37	3.78	4.01
Y_2O_3	2.71	0.59	0.98	0.67	0.75	1.12	4.13	3.33	3.46	3.24	4.69	3.79
La_2O_3	13.91	14.30	14.26	14.36	14.54	15.00	13.34	12.22	12.85	12.33	12.06	13.03
Ce_2O_3	24.80	27.09	28.49	28.59	27.15	28.84	25.15	22.07	22.81	22.74	21.51	22.68
Pr_2O_3	3.55	3.98	3.91	4.21	4.07	4.08	3.80	3.89	3.86	3.67	3.70	3.48
Nd_2O_3	13.86	15.13	15.43	15.18	15.48	15.04	13.59	14.93	13.41	15.04	14.73	13.09
Sm_2O_3	2.56	2.89	2.89	2.60	2.81	2.76	2.66	3.22	2.46	3.32	3.21	2.51
Gd_2O_3	2.01	1.76	1.59	1.39	1.52	1.53	2.21	2.69	1.97	2.86	2.79	2.28
Dy_2O_3	0.61	0.28	0.21	0.12	0.19	0.18	0.86	1.02	0.75	0.90	0.96	0.78
Er_2O_3	0.00	0.00	0.00	0.00	0.00	0.00	0.01	0.02	0.00	0.00	0.00	0.01
CaO	1.08	0.91	0.85	0.75	0.64	0.74	1.13	0.97	1.24	0.99	1.03	1.16
PbO	0.20	0.18	0.15	0.13	0.13	0.13	0.21	0.21	0.23	0.19	0.21	0.23
P_2O_5	27.28	27.87	27.90	27.74	27.83	28.05	27.78	26.94	27.29	27.43	26.74	27.23
Total	97.864	98.681	100.875	99.438	98.094	100.963	100.180	96.377	96.394	97.558	96.991	95.889
Age (Ma)	594	571	596	624	705	620	609	588	588	553	568	596
+/- (Ma)	42	47	56	66	75	68	42	41	36	41	38	37

Analyses no.	b1.13	b1.14	b1.15	b2.2	b2.3	b3.2	b3.3	b3.4	b3.5	b3.7	b3.9
Mode of occurrence	Inclusion in Bt										
SiO_2	0.06	0.06	0.06	0.10	0.07	0.06	0.27	0.28	0.24	0.22	0.16
UO_2	1.24	1.06	1.50	1.51	1.05	1.18	0.59	0.59	0.51	0.99	1.51
ThO_2	4.39	4.58	4.59	4.20	4.51	4.78	5.14	5.09	4.77	5.49	4.47
Y_2O_3	3.59	2.64	3.51	3.22	2.80	2.43	0.00	0.27	0.00	2.13	3.34
La_2O_3	13.02	13.29	13.22	12.74	12.96	13.80	14.78	15.03	13.92	14.10	13.39
Ce_2O_3	23.25	23.26	22.79	24.10	23.49	23.01	25.14	25.08	26.24	23.17	23.04
Pr_2O_3	3.68	3.73	3.75	3.80	3.85	3.67	4.12	3.84	3.93	3.68	3.72
Nd_2O_3	13.63	13.73	13.75	13.62	13.93	13.88	14.80	14.64	15.21	14.19	13.13
Sm_2O_3	2.68	2.68	2.62	2.58	2.84	2.51	2.33	2.20	2.52	2.28	2.48
Gd_2O_3	2.34	2.38	2.18	2.46	2.53	1.68	0.92	0.99	1.12	1.49	1.92
Dy_2O_3	0.98	0.81	0.91	0.82	0.78	0.46	0.10	0.08	0.06	0.40	0.70
Er_2O_3	0.07	0.02	0.00	0.00	0.00	0.00	0.00	0.00	0.00	0.00	0.03
CaO	1.17	1.16	1.22	1.15	1.09	1.11	0.92	0.99	1.05	1.21	1.14
PbO	0.21	0.19	0.24	0.22	0.20	0.21	0.18	0.19	0.17	0.22	0.23
P_2O_5	27.59	27.63	27.05	26.90	26.74	26.36	26.61	26.46	27.61	26.29	26.49
Total	97.900	97.225	97.384	97.410	96.830	95.129	95.894	95.734	97.348	95.849	95.751
Age (Ma)	585	555	583	550	578	569	604	636	620	596	565
+/- (Ma)	39	41	35	36	41	38	45	46	50	37	35

sillimanite presumably inverted from kyanite. On the other hand, the only aluminosilicate mineral included in the garnet mantle is sillimanite. Staurolite in the garnet mantle indicates that the growth of the garnet occurred in its stability field. The chemical zoning of garnet is well defined by an increase in X_{Mg} and a decrease in Mn from the core to the mantle, whereas Ca is almost constant. Therefore, the zoning pattern and inclusion minerals suggest prograde metamorphism occurred from the kyanite to the sillimanite stability field. The occurrence of relict kyanite next to sillimanite in the garnet core might suggest that the prograde *P-T* conditions are close to those of

Table 2. (Continued)

Analyses no.	b4.2	b4.4	b5.1	b5.2	b5.3	b5.4	b5.5
Mode of occurrence	In matrix						
SiO_2	0.24	0.20	0.14	0.18	0.28	0.22	0.15
UO_2	0.55	0.59	1.30	1.39	0.79	0.78	1.11
ThO_2	4.03	4.15	2.39	3.86	5.36	3.72	4.52
Y_2O_3	0.00	0.92	2.43	2.30	1.30	0.75	3.60
La_2O_3	14.95	14.77	13.37	13.83	15.01	14.36	12.71
Ce_2O_3	25.03	24.80	24.81	23.58	26.42	26.90	23.71
Pr_2O_3	3.92	3.95	3.67	3.79	3.95	3.68	3.66
Nd_2O_3	14.65	15.10	14.21	13.84	13.96	14.83	14.21
Sm_2O_3	2.47	2.46	2.68	2.76	2.07	2.56	2.56
Gd_2O_3	1.61	1.30	2.54	2.13	1.23	1.78	2.16
Dy_2O_3	0.27	0.19	0.87	0.75	0.20	0.37	0.78
Er_2O_3	0.00	0.00	0.00	0.01	0.00	0.00	0.02
CaO	0.77	0.88	0.69	0.98	1.22	0.87	1.18
PbO	0.19	0.20	0.16	0.20	0.21	0.23	0.20
P_2O_5	26.88	26.78	27.47	26.81	27.30	27.91	27.86
Total	95.541	96.285	96.720	96.392	99.290	98.954	98.421
Age (Ma)	742	757	568	567	615	831	567
+/- (Ma)	56	54	51	40	41	53	40

Analyses no.	b6.1	b6.2	b6.3	b6.4	b6.5	p1.1	p1.5
Mode of occurrence	In matrix					Inclusion in Pl	
SiO_2	0.31	0.21	0.19	0.20	0.31	0.26	0.25
UO_2	1.35	1.04	1.14	0.52	0.37	0.99	1.08
ThO_2	4.58	4.83	4.62	3.77	3.23	5.18	5.45
Y_2O_3	3.69	2.49	4.31	0.81	1.33	0.97	2.63
La_2O_3	12.61	13.62	12.93	14.77	14.73	13.89	13.68
Ce_2O_3	25.84	29.37	29.56	25.90	28.25	26.30	22.22
Pr_2O_3	3.73	3.75	3.63	4.07	4.00	3.54	3.78
Nd_2O_3	13.65	14.12	13.73	14.83	14.42	13.86	14.13
Sm_2O_3	2.49	2.54	2.65	2.69	2.65	2.47	2.46
Gd_2O_3	2.43	1.70	2.38	1.54	1.92	1.57	1.49
Dy_2O_3	0.78	0.52	0.70	0.31	0.51	0.36	0.44
Er_2O_3	0.00	0.00	0.00	0.00	0.00	0.00	0.00
CaO	1.28	1.35	1.40	0.81	0.71	1.29	1.25
PbO	0.21	0.23	0.20	0.18	0.15	0.22	0.23
P_2O_5	28.11	24.12	23.41	26.68	28.07	27.64	26.13
Total	101.062	99.871	100.862	97.086	100.651	98.540	95.216
Age (Ma)	539	638	570	777	787	622	604
+/- (Ma)	37	40	39	60	73	39	36

the kyanite–sillimanite transition, which is consistent with geothermobarometric estimates (Fig. 12 and Table 3). The estimated peak conditions (700 °C and 5.6 kbar) are higher than those of pelitic gneiss in southern Mefjell (550 °C, 4.5 kbar) (Osanai et al., 2013). The trend of decompression and cooling process is similar to those inferred for the Units D and D' in the SW-terrane (Osanai et al., 2013).

U–Th–Pb dating of monazite grains yields the range of ages between ca. 700–540 Ma (a weighted mean age of 587 Ma). Although, this age range of 700–540 Ma is too wide to constrain the precise timing of monazite forma-

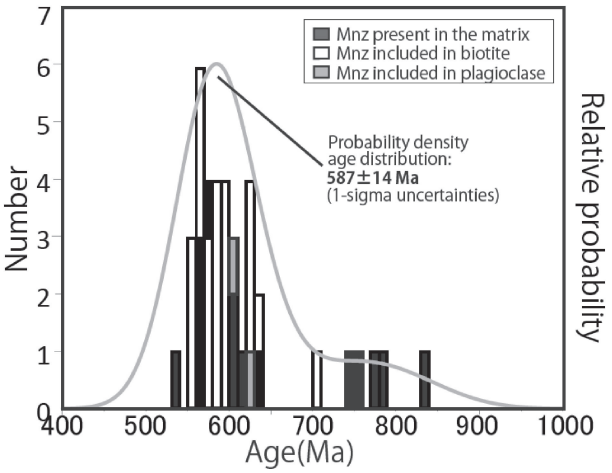

Figure 11. Histograms of electron microprobe chemical U-Th-Pb ages of monazite present in the matrix and included in biotite or plagioclase.

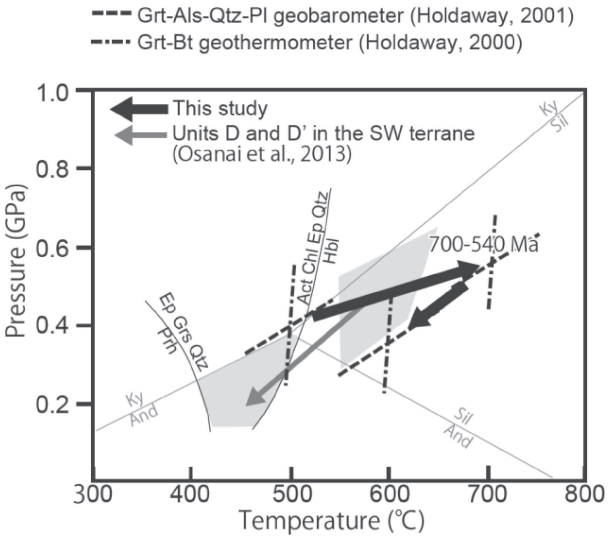

Figure 12. Pressure Temperature diagram showing the metamorphic conditions and *P-T-t* path inferred from the garnet porphyroblast. Black arrows are the *P-T* path deduced from the textual observations and thermobarometric calculations. Summary of the *P-T* conditions and retrograde *P-T* path of the Units D and D' in the SW terrane are also shown (grey areas and dark grey arrow; Osanai et al., 2013). The Al_2SiO_5 stability fields are after Holdaway (1971).

tion associated with metamorphism, it is consistent with the timing of the granulite-facies metamorphism proposed for the central and northeastern part of the SRM (650-600 Ma, e.g., Osanai et al., 2013), and also with the timing of the amphibolite- to greenschist-facies metamorphism for the southern and southwestern part of the SRM (590-530 Ma, e.g., Osanai et al., 2013). This 700-540 Ma age range obtained from the monazite in this study might be somehow be related to the long-lived (~ 150 my) igneous activity throughout the SRM (Elburg et al., 2016).

According to Osanai et al. (2013), most of the metamorphic rocks in Unit D yielded 590-530 Ma, and the 650-600 Ma metamorphic age is not common in Unit D. Thus, the range of the metamorphic ages between 700-540 Ma obtained from the metapelite sample in Mefjell of this study is significantly longer than those previously reported from Unit D. The inferred prograde metamorphism in this study with a slight increase in pressure might be related to subduction and/or tectonic loading during collision tectonics. This presumably supports the collision tectonic model proposed by Osanai et al. (2013) of which the NE terrane of the SRM has been thrust-faulted over the SW terrane during the period of 650-600 Ma. Our results presented here might provide some additional constraints on the metamorphism of the subducted SW terrane and further on the continental collision processes related to the amalgamation of Gondwana.

CONCLUSIONS

A garnet porphyroblast preserving both prograde and retrograde zonings is found in a metapelite from Mefjell, Sør Rondane Mountains. The garnet core contains kyanite as a relic inclusion, next to sillimanite. On the basis of textual observations and thermobarometric calculations, the garnet is interpreted to have formed during prograde metamorphism that passed through the kyanite stability field to the sillimanite stability field, and reached near peak metamorphic conditions (700 °C, 5.6 kbar) followed by retrogression (620 °C, 4.2 kbar). Monazite ages obtained from the metapelite yield the range of ages between ca. 700-540 Ma. The newly recognized prograde metamorphism and a wide range of monazite ages of the metapelite in Mefjell, might provide some additional constrains on the metamorphic evolution process during collision tectonics of the SRM proposed by Osanai et al. (2013).

Table 3. Thermobarometric results for Grt-Bt and Grt-Als-Pl-Qtz associations

Metamorphic Stage	Grt	Als	Bt	Pl	GB (°C)		GASP (kbar)	
					3 kbar	6 kbar	500 °C	700 °C
Pre-peak	Core	Ky or Sil	In Grt core	In Grt core	498	505	4.1	7.9
Peak	Mantle	Sil	Core (in the matrix)	Core (in the matrix)	703	712	5.2	8.3
Retrograde	Rim	Sil	In contact with Grt	Rim (in the matrix)	597	606	3.9	7.1

ACKNOWLEDGMENTS

We acknowledge Dr. Ikeda and an anonymous reviewer for constructive reviews and Prof. Owada for editorial efforts. We would like to thank all the members of the 51st Japanese Antarctic Research Expedition for their great supports and helps. We also thank Dr. Komiya and Dr. Yamamoto for analytical support at the University of Tokyo. We would like to greatly appreciate Mr. Negishi for analytical support with the X-ray mapping at Instrumental Analysis Center, Yokohama National University.

SUPPLEMENTARY MATERIALS

Color version of Figure 2 is available online from http://doi.org/10.2465/jmps.160919.

REFERENCES

Adachi, T. (2010) Metamorphic evolution and its implication for tectonic process in the central Sør Rondane Mountains, East Antarctica. pp 264, Ph.D. thesis, The Graduate University for Advanced Studies, Tokyo, Japan.

Adachi, T., Hokada, T., Osanai, Y., Nakano, N., Baba, S. and Toyoshima, T. (2013) Contrasting metamorphic records and their implications for tectonic process in the central Sør Rondane Mountains, eastern Dronning Maud Land, East Antarctica. In Antarctica and Supercontinent Evolution (Harley, S.L., Fitzsimons, I.C.W. and Zhao, Y. Eds.). Geological Society of London, Special Publications, 383, 113-133.

Asami, M., Osanai, Y., Shiraishi, K. and Makimoto, H. (1992) Metamorphic evolution of the Sør Rondane Mountains, East Antarctica. In, Recent Progress in Antarctic Earth Science (Yoshida, Y., Kaminuma, K. and Shiraishi, K. Eds.). TERRAPUB, Tokyo, 7-15.

Asami, M., Grew, E.S. and Makimoto, H. (2007) Relict sapphirine+kyanite associations in pyropic garnet from the eastern Sør Rondane Mountains, East Antarctica. Lithos, 93, 107-125.

Baba, S., Osanai, Y., Nakano, N., Owada, M., Hokada, T., Horie, K., Adachi, T. and Toyoshima, T. (2013) Counterclockwise *P-T* path and isobaric cooling of metapelites in Brattnipene, Sør Rondane Mountains, East Antarctica: implications for a tectonothermal event at the proto-Gondwana margin. Precambrian Research, 234, 210-228.

Elburg, M., Andersen, T., Jacobs, J., Läufer, A., Ruppel, A., Krohne, N. and Damaske, D. (2016) One hundred fifty million years of intrusive activity in the Sør Rondane Mountains (East Antarctica): implications for Gondwana assembly. The Journal of Geology, 124, 1-26.

Grantham, G.H., Macey, P.H., Horie, K., Kawakami, T., Ishikawa, M., Satish-Kumar, M., Tsuchiya, N., Graser, P. and Azevedo, S. (2013) Comparison of the metamorphic history of the Monapo Complex, northern Mozambique and Balchenfjella and Austhameren areas, Sør Rondane, Antarctica: Implications for the Kuunga Orogeny and the amalgamation of N and S. Gondwana. Precambrian Research, 234, 85-135.

Grantham, G.H., Macey, P.H., Ingram, B.A., Roberts, M.P., Armstrong, R.A., Hokada, T., Shiraishi, K., Jackson, C., Bisnath, A. and Manhica, V. (2008). Terrane correlation between Antarctica, Mozambique and Sri Lanka; comparisons of geochronology, lithology, structure and Metamorphism and possible implications for the geology of southern Africa and Antarctica. In GeodynamicEvolution of East Antarctica: A Key to the East-West Gondwana Connection (Satish-Kumar, M., Motoyoshi, Y., Osanai, Y., Hiroi, Y. and Shiraishi, K. Eds.). Geological Society of London, Special Publications, 308, 91-119.

Higashino, F., Kawakami, T., Satish-Kumar, M., Ishikawa, M., Maki, K., Tsuchiya, N., Grantham, G. and Hirata, T. (2013) Chlorite-rich fluid or melt activity during granulite facies metamorphism in the Late Proterozoic to Cambrian continental collision zone-An example from the Sør Rondane Mountains, East Antarctica. Precambrian Research, 234, 229-246.

Hokada, T. and Motoyoshi, Y. (2006) Electron microprobe technique for U-Th-Pb and REE chemistry of monazite, and its implications for pre-, peak- and post-metamorphic events of the Lützow-Holm Complex and the Napier Complex, East Antarctica. Polar Geoscience, 19, 118-151.

Holdaway, M.J. (1971) Stability of andalusite and the aluminum silicate phase diagram. American Journal of Science, 271, 2, 97-131.

Holdaway, M.J. (2000) Application of new experimental and garnet Margules data to the garnet-biotite geothermometer. American mineralogist, 85, 881-892.

Holdaway, M.J. (2001) Recalibration of the GASP geobarometer in light of recent garnet and plagioclase activity models and versions of the garnet-biotite geothermometer. American Mineralogist, 86, 1117-1129.

Jacobs, J., Elburg, M., Läufer, A., Kleinhanns, I., Henjes-Kunst, F., Estrada, S., Ruppel, S., Damaske, D., Montero, P. and Bea, F. (2015) Two distinct Late Mesoproterozoic/Early Neoproterozoic basement provinces in central/eastern Dronning Maud Land, East Antarctica: The missing link, 15-21°E. Precambrian Research, 265, 249-272.

Jacobs, J. and Thomas, R.J. (2004) Himalayan-type indenter-escape tectonics model for the southern part of the Neoproterozoic-early Paleozoic East African-Antarctic orogen. Geology, 32, 721-724.

Kawakami, T., Higashino, F., Skrzypek, E., Satish-Kumar, M., Grantham, G., Tsuchiya, N., Ishikawa, M., Sakata, S. and Hirata, T. (2017) Prograde infiltration of Cl-rich fluid into the granulitic continental crust from a collision zone in East Antarctica (Perlebandet, Sør Rondane Mountains). Lithos, 274-275, 73-92.

Kawakami, T., Satish-Kumar, M., Tsuchiya, N., Ishikawa, M., Higashino, F., Grantham, G. and Yoshida, K. (2010) Pelitic metamorphic rocks from Perlebandet and Balchenfjella, Sør Rondane Mountains, East Antarctica. Abstracts with Symposium on Polar Geosciences, GO008.

Kretz, R. (1983) Symbols for rock-forming minerals. American Mineralogist, 68, 277-279.

Meert, J.G. (2003) A synopsis of events related to the assembly of eastern Gondwana. Tectonophysics, 362, 1-40.

Nakano, N., Osanai, Y., Baba, S., Adachi, T., Hokada, T. and Toyoshima, T. (2011) Inferred ultrahigh-temperature metamorphism of amphibolitized olivine granulite from the Sør Rondane Mountains, East Antarctica. Polar Science, 5, 345-359.

Osanai, Y., Shiraishi, K., Takahashi, Y., Ishizuka, H., Tainosho, Y., Tsuchiya, N., Sakiyama, T. and Kodama, S. (1992) Geochemical characteristics of metamorphic rocks from the central Sør

Rondane Mountains, East Antarctica. In Recent Progress in Antarctic Earth Science (Yoshida, M., Kaminuma, K. and Shiraishi, K. Eds.). Terra, Tokyo, 17–27.

Osanai, Y., Nogi, Y., Baba, S., Nakano, N., Adachi, T., Hokada, T., Toyoshima, T., Owada, M., Satish-Kumar, M., Kamei, A. and Kitano, I. (2013) Geologic evolution of the Sør Rondane Mountains, East Antarctica: Collision tectonics proposed based on metamorphic processes and magnetic anomalies. Precambrian Research, 234, 8–29.

Owada, M. Sato, A., Osanai, Y., Toyoshima, T. and Shiraishi, K. (2008) Metamorphic processes of pelitic rocks at the deeper part of continental collision zone, Sør Rondane Mountains, East Antarctica. The Abstracts with Program 2008 Annual Meetting of Japan Association of Mineralogical Sciences, R3–11.

Shiraishi, K., Dunkley, D.J., Hokada, T., Fanning, C.M., Kagami, H. and Hamamoto, T. (2008) Geochronological constraints on the Late Proterozoic to Cambrian crustal evolution of eastern Dronning Maud Land, East Antarctica: a synthesis of SHRIMP U–Pb age and Nd model age data. In Geodynamic Evolution of East Antarctica: A Key to the East–West Gondwana Connection (Satish-Kumar, M., Motoyoshi, Y., Osanai, Y., Hiroi, Y. and Shiraishi, K. Eds). Geological Society of London, Special Publications, 308, 21–67.

Tsuchiya, N., Ishikawa, M., Satish-Kumar, M., Kawakami, T., Kojima, H., Kaiden, H., Miura, H., Suganuma, Y., Abe, M., Sasaki, D., Chiba, M., Okada, Y., Hashizume, F., Grantham, G. and Goderis, S. (2012) Report on geological, Geomorphological and meteorite fieldwork in the Sør Rondane Mountains, Eastern Dronning Maud Land, 2009–2010 (JARE–51). Antarctica Record, 56, 3, 295–379.

Manuscript received September 19, 2016
Manuscript accepted February 28, 2017

Manuscript handled by Masaaki Owada